JOURNAL OF MATERIALS SCIENCE 33 (1998) 1227–1232

Phenomenological investigation of inhomogeneities in Nd^{3+}-doped $Ba_2NaNb_5O_{15}$ single-crystal fibres grown by the laser-heated pedestal growth technique

M. FERRIOL, G. FOULON, A. BRENIER, G. BOULON
Laboratoire de Physico-Chimie des Matériaux Luminescents, Unite Mixtede Recherche CNRS 5620, Bâtiment 205, Université Claude Bernard Lyon-I, 43, boulevard, du 11 Novembre 1918, 69622 Villeurbanne Cédex, France

Inhomogeneities in $Ba_2NaNb_5O_{15}$ (BNN) single-crystal fibres undoped or doped with 1–5 at% Nd^{3+} and grown by the laser-heated pedestal growth technique were investigated by energy-dispersive X-ray microprobe analysis (EDXA), second-harmonic generation (SHG) measurements and interference contrast microscopy after chemical etching. The observed internal morphology of BNN fibres was correlated to SHG and EDXA measurements and involves convective flow instabilities in the molten zone and possibly unsteady interface kinetics. From this study, it appears that for a doping concentration equal to 3 at% Nd^{3+}, no growth striations nor any kind of inhomogeneity could be detected, indicating, as also shown by differential thermal analysis, that this mixture congruently melts, ensuring very-high-optical-quality crystals are obtained as no cracks nor microtwins are also present for this amount of neodymium. © *1998 Chapman & Hall*

1. Introduction

Among the most efficient materials for green second-harmonic generation (SHG), $Ba_2NaNb_5O_{15}$ (BNN) appears to have the highest non-linear coefficients [1] combined with no photorefractive damage [2, 3] as a result of its tungsten bronze-type structure [4]. However, industrial applications of BNN (SHG and laser oscillation) have not been made because the production of single crystals with sufficient crystalline quality has not yet been successful.

One of the major drawbacks of BNN is the occurrence of cracks during the cooling process of crystals grown by the Czochralski technique. Cracking is due to the large thermal expansion of the *c*-axis at the ferroelectric transition temperature [5]. Moreover, BNN crystals exhibit microtwins because of the exchange of *a* and *b* axes of the slightly orthorhombic crystallographic structure [4]. As microtwinning disturbs the optical properties, crystals should be detwinned by cooling under a compressive stress and simultaneously, poled under a direct-current voltage [3]. The necessity of such a procedure which sometimes leads to breaking of the crystals has also constituted an impediment for the commercial development of BNN.

Using previous results [6–8] indicating the positive influence of rare-earth doping on the cracking problem, we have shown in a recent article [9] that the addition of more than 1.5 mol% Nd_2O_3 enabled us to obtain, by the laser-heated pedestal growth technique (LHPG) [10, 11], uncracked crystals with a tetragonal tungsten bronze-type structure, avoiding therefore the occurrence of microtwins and leading to an important improvement in the crystalline quality.

Nevertheless, the purpose of this article is to investigate more closely the relationships between the internal morphology of the pulled fibres and their optical properties (green-light SHG).

2. Experimental procedure

BNN source rods were obtained using a conventional ceramic processing technique. Nb_2O_5 (purity 99.95%; optical grade), $Ba(NO_3)_2$ (purity, 99.99%) and Na_2CO_3 (purity 99.99%) from Cerac were thoroughly mixed in a ball mill. The resulting powder was then cold pressed under 3000 kg cm^{-2} into discs which were placed in alumina crucibles and fired at 1250 °C for 15 h in an oxygen flow under 1 bar pressure. Completion of the reaction was checked by X-ray powder diffractometry. Doped BNN was made by grinding and mixing the BNN powder with Nd_2O_3 (purity, 99.999%; Cerac).

The feedings rods of doped BNN were then obtained by grinding the powder mixed with 0.5% of a briquetting agent (Chemplex Spectroblend powder) and cold pressing it into discs 25 mm in diameter and

3–5 mm in thickness. The pellets were finally sintered at 650 °C for 2 h and at 1250 °C for 8 h. After cooling, they were cut into square rods between 1 mm × 1 mm and 2 mm × 2 mm.

Quantitative analyses for Na, Ba and Nb along the pulled fibres were performed by X-ray energy dispersion (JEOL 840 ALGS microscope; EDX Tracor microprobe) taking the intensities of K lines for Na and of L lines for Ba and Nb (accelerating voltage, 15 kV; take-off angle, 40°; *ZAF* correction, where Z is the atomic number, A the absorption correction factor and F the fluorescence correction factor. Measurements were obtained within an accuracy of 2%.

The internal morphology of the as-grown fibres was examined by interference contrast microscopy (Leica DMR-RXE) after embedding in epoxy resin, mechanical polishing and etching with commercial concentrated fluorhydric acid at room temperature for 30–40 min or with a $HF–HNO_3$ mixture (1:2 by volume of commercial concentrated acids) at 80 °C for 10 min.

SHG experiments were performed with a dye laser (Laser Analytical Systems) pumped by a frequency-doubled Nd-doped yittrium aluminium garnet laser (BM Industries). The detection of the SHG signal was carried out with a Jobin–Yvon JYHRS-2 monochromator, a Hamamatsu R-1767 photomultiplier and a Stanford SRS-250 boxcar averager.

3. Results

Several *b*-axis (pulling with an oriented seed) or randomly (pulling with a ceramic seed) oriented BNN single-crystal fibres undoped or doped with 1, 2, 3, 4 and 5 at% Nd^{3+} were grown in air atmosphere with pulling rates between 30 and 40 mm h^{-1} and diameters in the range 400–800 μm. Our LHPG set-up has been described elsewhere [12].

A set of crystals corresponding to a doping level equal to 1, 3, 4 and 5 at% Nd^{3+} was used for SHG measurements whereas another set of fibres corresponding to a doping level of 0, 1, 3, 4, and 5 at% Nd^{3+} was embedded in epoxy resin, polished and etched before microscopic observation. In either case, the single-crystal character was checked under the polarizing microscope.

EDXA showed no variation in composition characteristic of some macrosegregation (effective distribution coefficients close to 1) all along the pulled fibres as shown by Fig. 1 obtained for a fibre doped with 4 at% Nd^{3+}. However, the rather large measured deviations, 1–2 wt% from the mean, can be interpreted as the result of some inhomogeneity on the microscopic scale.

The non-critical phase-matching curves at room temperature are given in Fig. 2. The variation in the maximum phase-matching wavelength with neodymium content shows the tunability of the material but, also, the curves reveal some inhomogeneity of the different studied fibres except for 3 at% Nd^{3+} for which a sharp peak was obtained.

Etching of the other set of fibres gave the following results which can be easily correlated to the observations made from SHG experiments. The *b*-axis-oriented fibres were always etched perpendicular to the *c* axis and no particular direction was chosen for randomly oriented fibres.

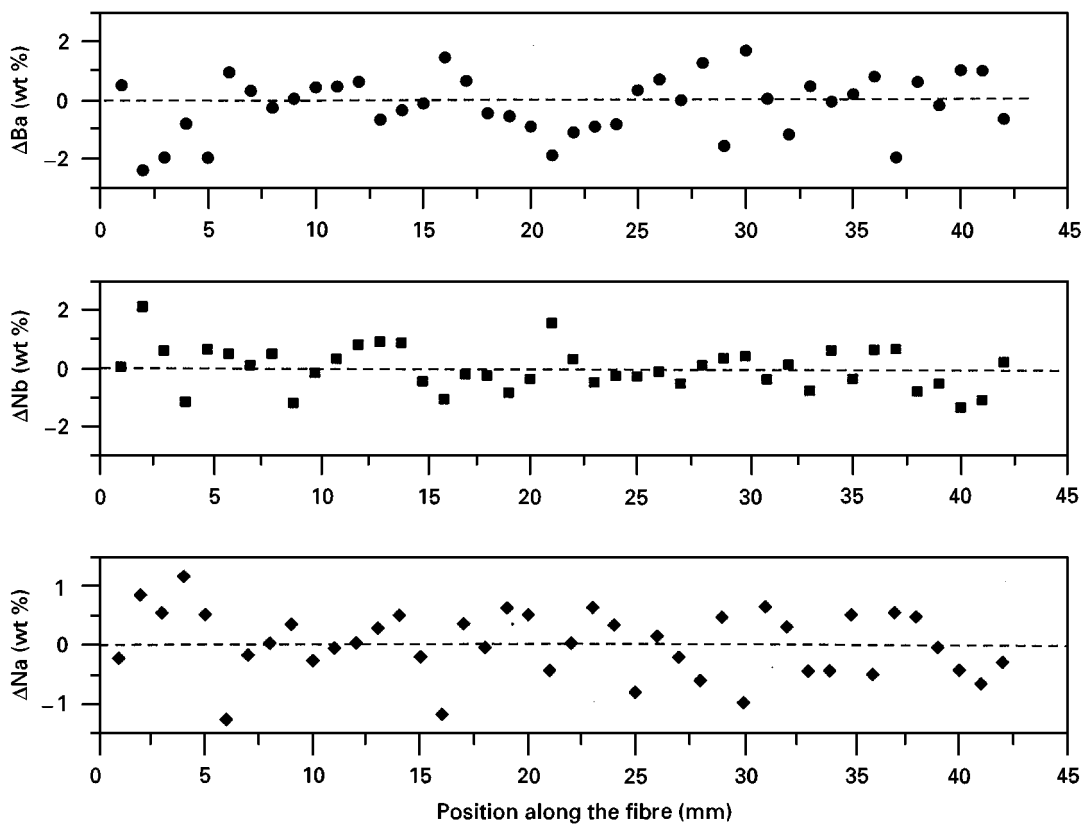

Figure 1 Variations in chemical composition along the growth axis of a 4 at% Nd^{3+}-doped BNN fiber (◆), Na; (■), Nb; (●), Ba.

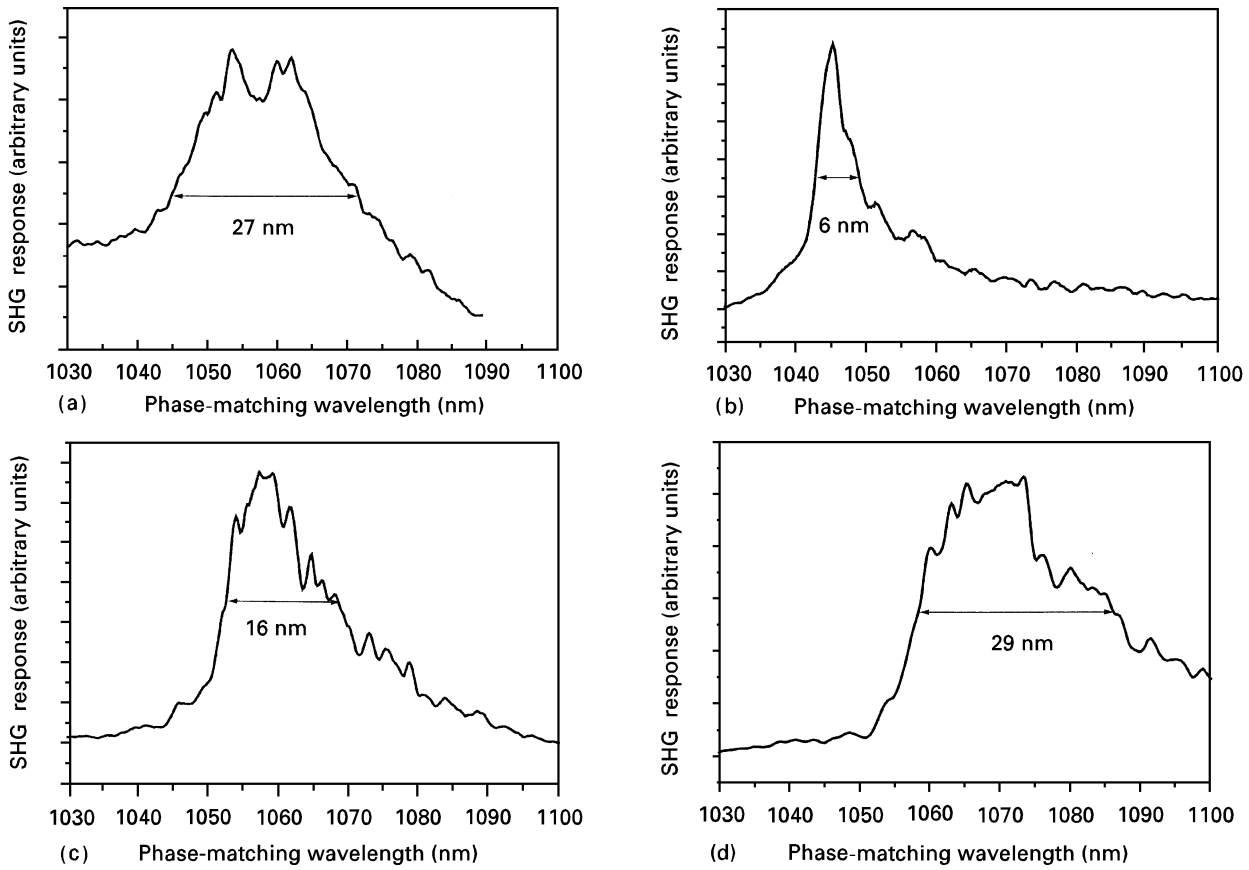

Figure 2 Non-critical phase-matching curves and full-width at half-maximum at room temperature of *b*-axis-oriented BNN fibres as a function of neodymium content: (a) 1 at% Nd^{3+}; (b) 3 at% Nd^{3+}; (c) 4 at% Nd^{3+}; (d) 5 at% Nd^{3+}.

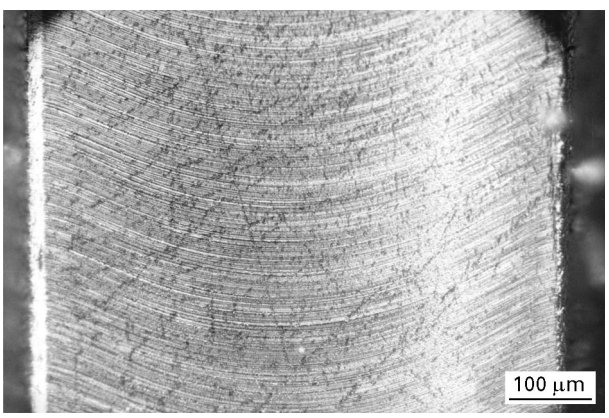

Figure 3 Internal morphology of an undoped randomly oriented BNN fibre after etching (growth direction: from the bottom to the top of the figure). (Magnification: 27×.)

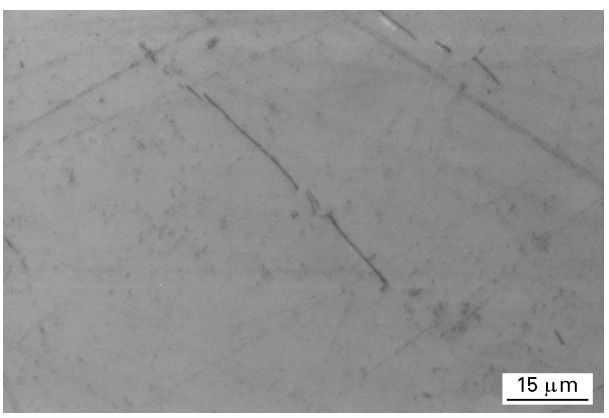

Figure 4 Internal morphology of a 3 at% Nd^{3+}-doped *b*-axis-oriented BNN fibre after etching (growth direction: from the bottom to the top of the figure). (Magnification: 175×.)

Besides the dislocation pits appearing at ferroelectric domain boundaries already mentioned [9], the internal morphology of an undoped randomly oriented BNN fibre is illustrated in Fig. 3. It shows rather regular striations following the curvature of the convex growth interface. The frequencies calculated from the striation spacings are in the range 1–2 Hz. A similar pattern was also obtained for a 1 at% Nd^{3+}-doped fibre.

For a doping concentration of 3 at% Nd^{3+} (*b*-axis-oriented fibre), etching revealed no apparent defects (Fig. 4).

For a *b*-axis-oriented fibre doped with 4 at% Nd^{3+} (Fig. 5), three different zones were observed. Fig. 5a shows a part of the first half of the fibre and the striations already observed with disappearance of these striations near the core region of the fibre. In Fig. 5b, corresponding to the second half of the fibre, no striations but one can observe step-like parallel rows inclined to the growth axis with an angle of about 65–70°. At the end of the fibre (Fig. 5c), no defects are observable as for 3 at% Nd^{3+}.

For a doping concentration of 5 at% Nd^{3+} (Fig. 6), three kinds of domain can be typically observed:

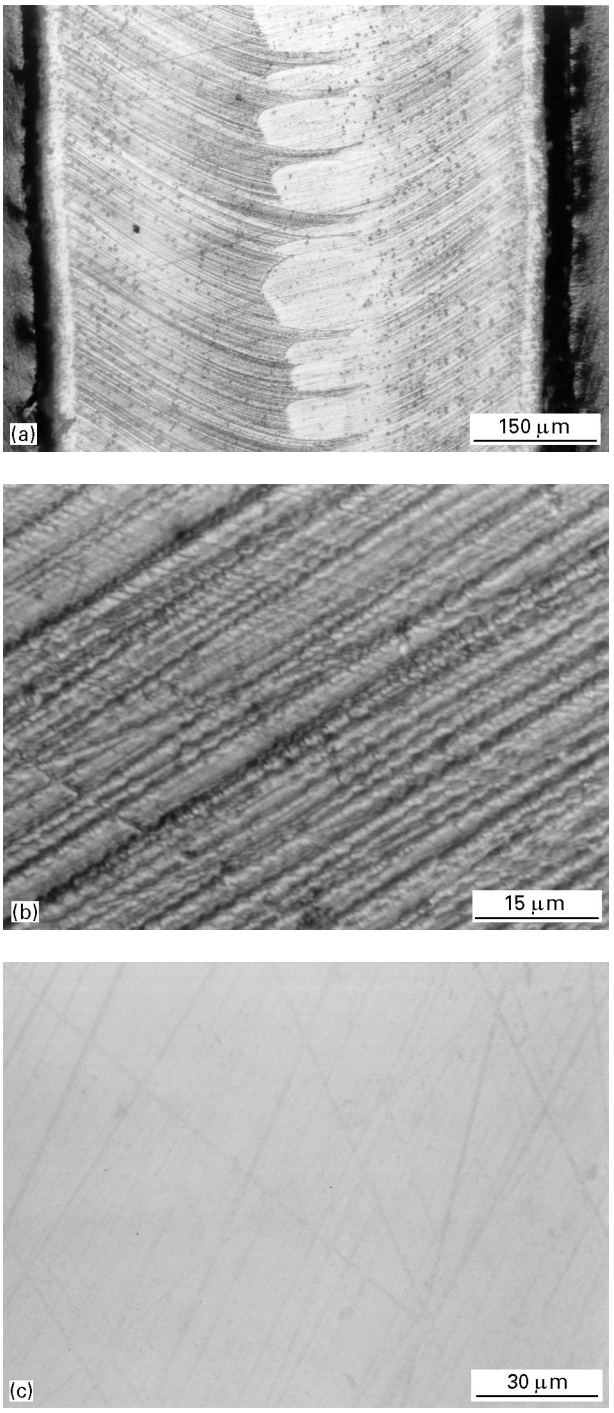

Figure 5 Internal morphology of a 4 at% Nd^{3+}-doped *b*-axis-oriented BNN fibre after etching (growth direction: from the bottom to the top of the figures): (a) first half of the fibre; (b) second half of the fibre; (c) end of the fibre. (Magnifications: (a) 26 ×; (b) 260 ×; (c) 130 ×.)

striations and a part free of striations (Fig. 6a; randomly oriented fibre), step-like parallel rows formed by the stacking of kinds of platelets with an edge length between 2 and 4 μm and inclined with the same angle as that observed in the case of the 4 at% Nd^{3+} fibre (Fig. 6b and 6c; randomly oriented fibre and *b*-axis-oriented fibre, respectively) and a zone in which rows and striations are superimposed as shown in Fig. 6d (*b*-axis-oriented fibre). Fig. 6a also shows a darker zone due to dislocations pits corresponding to ferroelectric domain boundaries as for undoped BNN. It

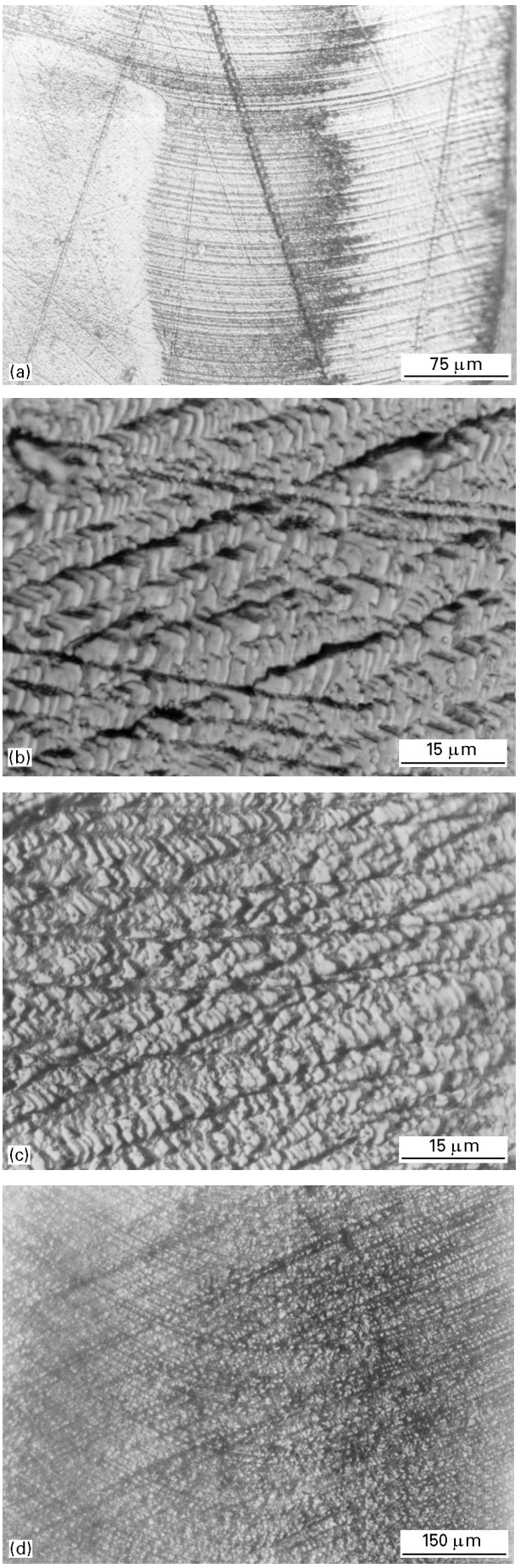

Figure 6 Internal morphology of a 5 at% Nd^{3+}-doped *b*-axis-oriented BNN fibre after etching (growth direction: from the bottom to the top of the figures): (a), (b) randomly oriented fibre; (c), (d) *b*-axis-oriented fibres. (Magnifications: (a) 52 ×; (b), (c) 260 ×; (d) 26 ×.)

is worth noting that for the other neodymium contents the fibres appeared as almost a single domain.

4. Discussion

Only strong perturbations of convective flows in the molten zone can explain the observed morphology of the BNN fibres shown in Figs 3, 5a and 6a.

Growth striations correspond to compositional fluctuations resulting from convective instabilities which affect both the heat and the species transport at the growth interface [13]. In the LHPG technique where the surface to volume ratio of the melt is very important and in the absence of rotation as is the case in our apparatus, convection is mainly driven by surface tension variations (Marangoni convection) [14]. When the characteristic Marangoni number [15]

$$\mathrm{Ma} = \rho_1 \left(-\frac{\partial \sigma}{\partial T} \right) (T_{\max} - T_m) \frac{r_m}{\mu^2}$$

with ρ_1 the melt density, σ the melt–vapour surface tension at temperature T, $T_{\max}$ the melt temperature where the melt is heated, T_m the melting temperature and μ the viscosity, exceeds a critical value Ma_c, the convection becomes oscillatory (time-dependent) perturbing heat and solute transport phenomena at the growth interface and striations parallel to the growth interface appear in the crystal. The frequencies estimated for the striations observed in our fibres (1–2 Hz) are in agreement with such behaviour. However, the lack of physical data about BNN melts does not allow us to estimate any value of Ma and our interpretation can only be qualitative. When the Marangoni number greatly exceeds Ma_c (possibly because of the increase in the neodymium content) the instability increases and the flow passes from an oscillatory to a chaotic state strongly perturbing the characteristic toroidal vortex of Marangoni convection and possibly allowing patterns such as those depicted in Figs 5a and 6a.

As growth striations can only occur when the liquid and the crystallizing solid have different compositions (non-congruent melting allowing microsegregation), the morphology observed for undoped BNN (Fig. 3) suggests that the stoichiometric compound $Ba_2NaNb_5O_{15}$ is not congruently melting, contrary to the results given by Scott *et al.* [16]. This is supported by the experimental observations of Barraclough *et al.* [17] on crystals pulled by the Czochralski technique. For these workers, the congruency would be obtained for the composition $Ba_{2.08}Na_{0.71}Nb_5O_{14.94}$, crystals with that composition appearing free of striations, whereas Carruthers and Grasso [18] found $Ba_{2.19}Na_{0.82}Nb_5O_{15.1}$. The non-congruent behaviour of stoichiometric BNN was confirmed by a differential thermal analysis (DTA) (TAG 24 Setaram apparatus). Fig. 7 shows the DTA trace obtained. Obviously the shape of the endothermic peak can only be attributed to the overlapping of two peaks corresponding to the crossing of the solidus (at 1440 °C) and liquidus (at 1456 °C) surfaces, respectively, of the BNN

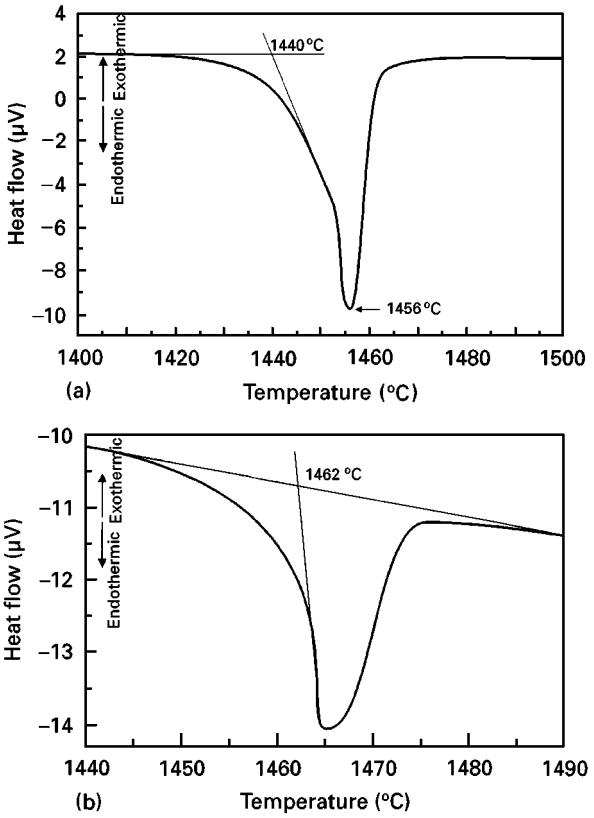

Figure 7 DTA of (a) undoped and (b) 3 at% Nd^{3+}-doped BNN samples (heating rate, 10 °C min^{-1}).

solid solution range in the $BaO–Na_2O–Nb_2O_5$ ternary system.

It should also be noted that the flatness of these solidus and liquidus surfaces [17] surely enhances the tendency to microsegregation (all other things being equal). This could be confirmed by the results obtained on $K_3Li_{2-x}Nb_{5+x}O_{15+2x}$ fibres with also a tungsten bronze-type structure for which slopes of the liquidus and solidus surfaces of the corresponding solid solution are steeper [19] and for which no striations were observed [20].

At the point of congruency, temperature fluctuations cannot alter the solidifying composition. Therefore, the DTA performed on a 3 at% Nd^{3+}-doped BNN sample (Fig. 7) and the absence of striations in the corresponding crystal (Fig. 4) allow us to conclude that melting is congruent for that composition.

The exact reason of the morphology shown in Figs 5b, 6b and 6c can hardly be attributed to convective flow instabilities. The phenomenon appears much more marked as the neodymium content increases and was not found in undoped or slightly doped BNN fibres. We have shown earlier from low-temperature spectroscopy measurements that Nd^{3+} ions occupy Ba^{2+} and Na^+ sites in the tungsten bronze-type structure of BNN [21] and could not substitute for Nb^{5+} ions owing to the larger ionic radius of Nd^{3+}. In these conditions, charge compensation can only be achieved by the creation of vacancies in the lattice. The observed morphology could therefore be linked to the difficulty for the host lattice to accommodate Nd^{3+} ions as the neodymium content increases.

The mechanism by which the observed inclined rows are created is not yet clear and the inclination is probably related to a particular crystallographic plane. Among the various origins of microscopic inhomogeneities [22], unsteady conditions due to the apparatus or pressure variations cannot be invoked in our set-up and, as unsteady convections or constitutional supercooling do not produce the patterns discussed above, unsteady interface kinetics with a stepped or terraced growth interface could possibly be involved [22]. In these conditions, the lateral growth at the edges of steps would be responsible for the inclination of the observed rows (Figs 5b, 6b and 6c). The pattern exhibited in Fig. 6d would therefore result from convective flow instabilities combined with unsteady interface kinetics. However, more complementary investigations are required and will be initiated soon.

5. Conclusion

Inhomogeneities in BNN single-crystal fibres undoped or doped with 1–5 at% Nd^{3+} observed by SHG measurements can be related to crystal internal morphology. It was investigated by interference contrast microscopy after chemical etching and mainly has its origin in instabilities of convective flows. To avoid striations, capillary convection (Marangoni effect) can be reduced by a reduction in the temperature and concentration gradients along the free melt surface. In this aim, two possibilities can be considered in our LHPG apparatus: use of an after-heater and/or change in the thermal conductivity of the growth atmosphere near the molten zone.

The morphology observed for doping concentrations higher than 3 at% and possibly related to the accommodation of Nd^{3+} ions by the host lattice could involve unsteady interface kinetics with a stepped growth interface to be confirmed by further investigations.

Finally, the doping concentration of 3 at% Nd^{3+} corresponds to a congruently melting mixture. This is important for the further growth of high-optical-quality BNN crystals since, beside the absence of cracks and twins due to the influence of rare-earth doping and to the tetragonal structure, the congruent melting will ensure no striations or microscopic inhomogeneities.

Acknowledgements

The authors wish to thank Professor Martin M. Fejer and Dr. Roger K. Route (Ginzton Laboratory, Stanford University, USA) for fruitful discussions during the writing of this article.

References

1. V. G. DMITRIEV, G. G. GURZDAYAN and D. N. NIKOGOSYAN, in "Handbook of nonlinear optical crystals" (Springer, Berlin, 1991).
2. J. E. GEUSIC, H. J. LEVINSTEIN, J. J. RUBIN, S. SINGH and L. G. VAN UITERT, *Appl. Phys. Lett.* **11** (1967) 269.
3. S. SINGH, D. A. DRAEGERT and J. E. GEUSIC, *Phys. Rev. B* **2** (1970) 2709.
4. P. B. JAMIESON, S. C. ABRAHAMS and J. L. BERNSTEIN, *J. Chem. Phys.* **50** (1969) 4352.
5. J. S. ABELL, K. G. BARRACLOUGH, I. R. HARRIS, A. W. VERE and B. COCKAYNE, *J. Mater. Sci.* **6** (1971) 1084.
6. J. L. MUKHERJEE, C. P. KHATTAK, K. P. GUPTA and F. F. YWANG, *J. Solid State Chem.* **24** (1978) 163.
7. M. SHIMAZU, M. TSUKIOKA, M. MITOBE, S. KUROIWA and S. TSUTSUMI, *J. Mater. Sci.* **25** (1990) 4525.
8. M. SHIMAZU, H. SHIUYA, S. KUROIWA, M. TSUKIOKA and S. TSUTSUMI, *Jpn. J. Appl. Phys.* **29** (1990) 2435.
9. G. FOULON, M. FERRIOL, A. BRENIER and G. BOULON, *Eur. J. Solid State Inorg. Chem.* **33** (1996) 673.
10. R. S. FEIGELSON, *Springer Ser. Opt. Sci.* **47** (1985) 129.
11. *Idem., J. Cryst. Growth* **79** (1986) 669.
12. G. FOULON, M. FERRIOL, A. BRENIER, M. T. COHEN-ADAD and G. BOULON, *Chem. Phys. Lett.* **245** (1995) 555.
13. G. MULLER and A. OSTROGORSKY, in "Handbook of crystal growth" (Elsevier, Amsterdam, 1994) p. 789.
14. M. M. FEJER, PhD thesis, Stanford University, California (1986).
15. C. E. CHANG and W. R. WILCOX, *J. Cryst. Growth* **28** (1975) 8.
16. B. A. SCOTT, E. A. GIESS and D. F. O'KANE, *J. Amer. Ceram. Soc.* **53** (1970) 14.
17. K. G. BARRACLOUGH, I. R. HARRIS, B. COCKAYNE, J. G. PLANT and A. W. VERE, *J. Mater. Sci.* **5** (1970) 389.
18. J. R. CARRUTHERS and M. GRASSO, *Mater. Res. Bull.* **4** (1969) 413.
19. B. A. SCOTT, E. A. GIESS, B. L. OLSON, G. BURNS, A. W. SMITH and D. F. O'KANE, *ibid.* **5** (1970) 47.
20. M. FERRIOL, G. FOULON, A. BRENIER, M. T. COHEN-ADAD and G. BOULON, *J. Cryst. Growth* **173** (1997) 226.
21. G. FOULON, A. BRENIER, M. FERRIOL, M. T. COHEN-ADAD and G. BOULON, *Chem. Phys. Lett.* **249** (1996) 381.
22. G. MULLER, in "Convection and inhomogeneities in crystal growth from the melt" (Springer, Berlin, 1988) p. 77.

Received 29 April
and accepted 24 September 1997